Int. J. Electrochem. Sci., 12 **(2017)** 8095 – 8105, doi: 10.20964/2017.09.25

International Journal of
ELECTROCHEMICAL
SCIENCE
www.electrochemsci.org

Structure and Delithiation/Lithiation of the Lithium-Rich Layered Oxide $Li[Li_{0.23}Ni_{0.15}Mn_{0.62}]O_2$ as Cathode Material

Jin-Xia Wang[1,3], *Rong-Min Gu*[1,3], *Yun-Peng Zhang*[1,3], *Bo-Jun Yu*[2,3], *Cheng-Yang Wang*[2,3],
Ming-Wei Li[1,3,*]

[1] Department of Chemistry, Tianjin University, Tianjin 300072, China
[2] Key Laboratory for Green Chemical Technology of Ministry of Education, School of Chemical Engineering and Technology, Tianjin University, Tianjin 300072, China
[3] Collaborative Innovation Center of Chemical Science and Engineering (Tianjin), Tianjin University, Tianjin 300072, China
[*] E-mail: mingweili@tju.edu.cn

Received: 29 April 2017 / *Accepted:* 5 July 2017 / *Published:* 13 August 2017

The typical lithium-rich layered oxide $Li[Li_{0.23}Ni_{0.15}Mn_{0.62}]O_2$ is synthesized via a solid state reaction, and is used as the cathode material for lithium-ion batteries. *In situ* X-ray diffraction analyses reveal the formation process of $Li[Li_{0.23}Ni_{0.15}Mn_{0.62}]O_2$ crystallites with $C2/m$ monoclinic symmetry. The $Li[Li_{0.23}Ni_{0.15}Mn_{0.62}]O_2$ cathode delivers an initial discharge capacity of 221 mAh g^{-1} and keeps a reversible capacity of 174 mAh g^{-1} after 50 cycles. A large capacity loss and the unique charge curve during the first cycle both indicate that $Li[Li_{0.23}Ni_{0.15}Mn_{0.62}]O_2$ was changed into $Ni_{0.2}Mn_{0.8}O_2$ due to irreversible oxygen loss and "rich lithium" extraction. The cathode's high capacity results from the reversible conversions between $Ni_{0.2}Mn_{0.8}O_2$ and $LiNi_{0.2}Mn_{0.8}O_2$. Both $Ni_{0.2}Mn_{0.8}O_2$ and $LiNi_{0.2}Mn_{0.8}O_2$ keep a stable framework during cycling due to two suggested reasons: (1) some transition metal atoms migrate into the lithium layers and play as the supports between the transition metal layers; (2) 1/4 Mn keeps a stable tetravalent state during cycling and then weakens the Jahn-Teller effect of Mn^{3+}. The predicted reversible capacity of $Li[Li_{(1-2x)/3}Ni_xMn_{(2-x)/3}]O_2$ $(0 < x < 0.5)$ increases from 229 to 280 mAh g^{-1} with increasing x value, and fairly coincides with the experimental results in this work and literature.

Keywords: Lithium-rich layered oxide; cathode; lithium-ion battery

1. INTRODUCTION

Lithium-rich layered oxide $Li[Li_{(1-2x)/3}Ni_xMn_{(2-x)/3}]O_2$ $(0 < x < 0.5)$ has attracted increasing attention as a potential alternative to the expensive $LiCoO_2$ cathode material for lithium-ion batteries [1−3]. Besides its low cost and high stability, $Li[Li_{(1-2x)/3}Ni_xMn_{(2-x)/3}]O_2$ often delivers a high capacity

(> 200 mAh g^{-1}) [4−7]. Lithium-rich layered oxide suffers from a unique capacity loss at a high charge voltage above 4.5 V *vs.* Li^+/Li. Simultaneously, its crystal structure is rearranged due to oxygen loss and lithium extraction.

Before the commercial applications of lithium-rich layered oxide as cathode material, it is important to understand its structure transformation and delithiation/lithiation mechanism.

Recently, we investigated electrochemical behavior of the typical lithium-rich layered oxide $Li[Li_{0.23}Ni_{0.15}Mn_{0.62}]O_2$, and suggested a lithium transfer mechanism to explain its performance during the initial charge [8]. $Li[Li_{0.23}Ni_{0.15}Mn_{0.62}]O_2$ is often written as $0.9Li[Li_{1/3}Mn_{2/3}]O_2{\cdot}0.4LiNi_{0.5}Mn_{0.5}O_2$ or $0.6Li_2MnO_3{\cdot}0.4LiNi_{0.5}Mn_{0.5}O_2$ to emphasize its two components $Li[Li_{1/3}Mn_{2/3}]O_2$ and $LiNi_{0.5}Mn_{0.5}O_2$ [9, 10]. Both components have a similar layered structure with an interlayer spacing of ~ 4.7 nm and may facilely form a solid solution.

According to our suggested mechanism, the predicted capacity of $xLi_2MnO_3{\cdot}(1-x)LiNi_{0.5}Mn_{0.5}O_2$ ($0 \leq x \leq 1$) increases from 230 to 280 mAh g^{-1} with x value increasing from 0 to 1, and fairly coincides with the reported results from literatures. Nevertheless, the roles of "rich lithium", Ni, and Mn are still ambiguous. Additionally, the crystal structure of $Li[Li_{0.23}Ni_{0.15}Mn_{0.62}]O_2$ and its transformation during cycling are closely related to its electrochemical behavior, and need further investigating.

In this work, we investigated the formation process of $Li[Li_{0.23}Ni_{0.15}Mn_{0.62}]O_2$ during a solid state reaction, and studied its structure evolution and lithium extraction/insertion mechanism. The investigation is helpful for understanding the high reversible capacity and cycle stability of lithium-rich layered oxide.

2. EXPERIMENTAL

The $Li[Li_{0.23}Ni_{0.15}Mn_{0.62}]O_2$ sample was synthesized by a stoichiometric mixture of Li_2CO_3, $MnCO_3$, and $NiCO_3$ via a solid state reaction at 900 °C for 8 hours. To select the reaction temperature and detect the phase transformation, we firstly measured the thermogravimetric analysis and differential scanning calorimetry (TG-DSC) of the mixture by a simultaneous thermal analyzer (STA 409 PC/PG, NETZSCH) from room temperature to 1000 °C. Secondly, an *in situ* X-ray diffractometer (XRD, D/Max-2200, Rigaku) using Cu $K\alpha$ radiation (λ = 0.15406 nm) was used to record the phase transformation from room temperature to 950 °C.

Electrochemical behavior of $Li[Li_{0.23}Ni_{0.15}Mn_{0.62}]O_2$ was tested within CR2430-type coin cells using lithium metal as the anodes. $Li[Li_{0.23}Ni_{0.15}Mn_{0.62}]O_2$, carbon black, and polyvinylidene fluoride (80/10/10 in weight) were mixed using N-methyl-2-pyrrolidone as a solvent, and pasted on aluminum foil to prepare the cathodes. 1.0 M $LiPF_6$ in ethylene carbonate-dimethyl carbonate (1/1 in volume) was used as the electrolyte. Polypropylene microporous film was used as the separator. Discharge/charge tests were performed between 2.0 and 4.8 V (*vs.* Li^+/Li) at a current density of 20 mA g^{-1}. Two cathodes from the coin cells after 20 discharges and 50th charges respectively were analyzed by XRD (PANalytical, Netherlands) using Cu $K\alpha$ radiation (λ = 0.15406 nm). Morphologies of the cycled cathode materials were recorded by a high-resolution transmission electron microscope (HRTEM, Tecnai G^2 F20, FEI).

3. RESULTS AND DISCUSSION

As shown in Fig. 1, the raw material has a total weight loss of 38.9% below 1000 °C, fairly coinciding with the theoretical weight loss (38.0%) of the carbonates as raw material. An endothermic peak appears at 858 °C with an enthalpy of ~ 52 J g^{-1} but with no weight loss. So there is a phase transition at 858 °C.

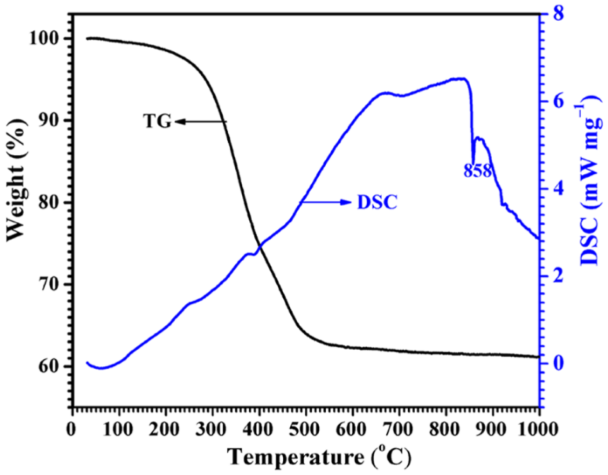

Figure 1. TG-DSC curves of the raw material, including stoichiometric Li_2CO_3, $NiCO_3$, and $MnCO_3$, for synthesizing $Li[Li_{0.23}Ni_{0.15}Mn_{0.62}]O_2$.

Fig. 2 shows the *in situ* XRD patterns recording the formation process of $Li[Li_{0.23}Ni_{0.15}Mn_{0.62}]O_2$ via a solid state reaction. It indicates that in the raw material both $MnCO_3$ and $NiCO_3$ are composed of trigonal phases (space group $R\bar{3}c$). They have the similar diffraction peaks at the neighbor 2θ degrees. Compared with $NiCO_3$, $MnCO_3$ shows diffraction peaks at lower 2θ degrees due to the larger size of Mn^{2+} ions. Li_2CO_3 has a monoclinic $C2/c$ structure. As the temperature increases to 500 °C, almost all diffraction peaks for $MnCO_3$ disappear, while there appear some new diffraction peaks, including the higher peak at ~ 44^{o}. At high temperatures, the peaks shift left due to the expansion of crystal lattices.

The crystal structure is crucial for understanding the electrochemical behavior of lithium-rich layered oxide. There ever were arguments about whether lithium-rich layered oxides mainly consist of a trigonal phase ($R\bar{3}m$) or a monoclinic phase ($C2/m$) [1, 3, 11−13]. Javis *et al*. [11] found that the conventional XRD only characterizes $Li[Li_{0.2}Ni_{0.2}Mn_{0.6}]O_2$ as either a monoclinic $C2/m$ phase or a combination of trigonal $R\bar{3}m$ phase and monoclinic $C2/m$ phase. They proved that $Li[Li_{0.2}Ni_{0.2}Mn_{0.6}]O_2$ is composed a solid solution with $C2/m$ monoclinic symmetry and multiple planar defects by aberration-corrected scanning transmission electron microscopy (STEM), diffraction scanning transmission electron microscopy, and electron diffraction. Recently, Shukla *et al.* [12] showed that the $Li[Li_{0.2}Ni_{0.13}Mn_{0.54}Co_{0.13}]O_2$ crystallites consist of a single monoclinic phase with a Co- and/or Ni-rich spinel structure surface by the help of STEM, electron energy loss spectroscopy (EELS), and X-ray energy-dispersive spectroscopy (XEDS). Herein, according to the ordered evolution and the diffraction peaks shown in Fig. 2, we suggested that the synthesized $Li[Li_{0.23}Ni_{0.15}Mn_{0.62}]O_2$ material is a solid solution with a monoclinic *C*2/*m* structure.

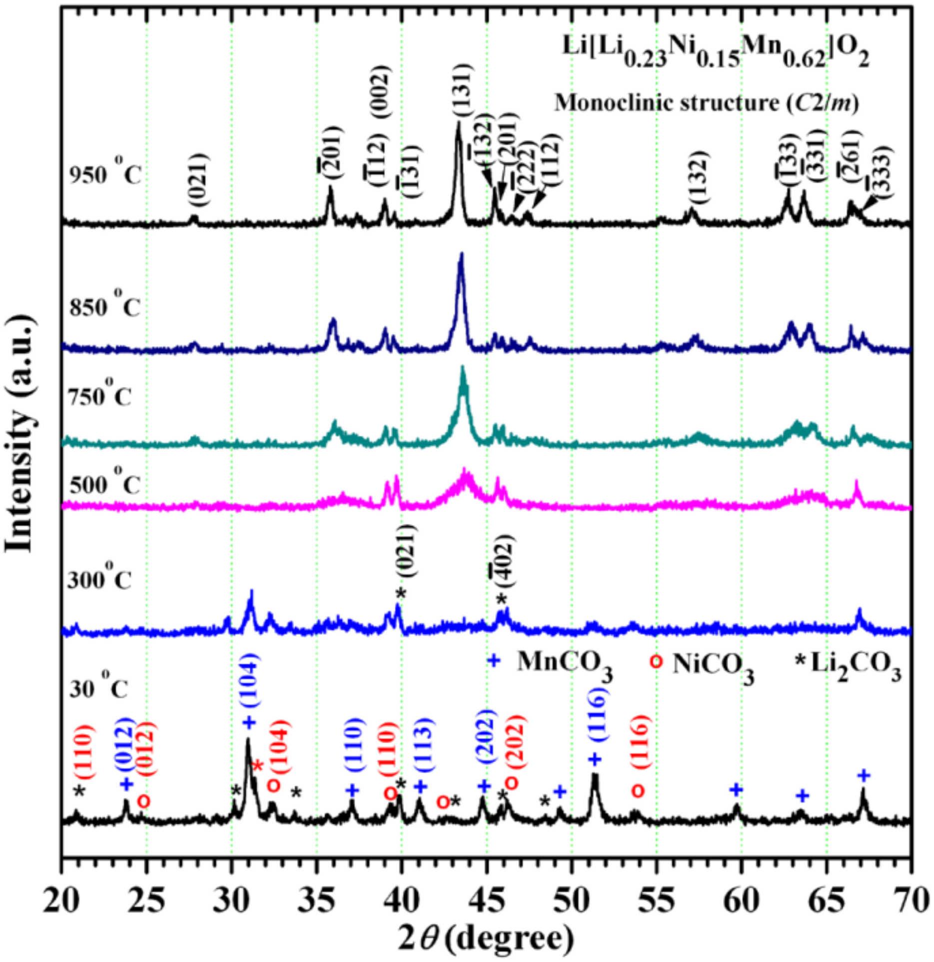

Figure 2. *In situ* XRD patterns showing the formation of monoclinic $Li[Li_{0.23}Ni_{0.15}Mn_{0.62}]O_2$ from the raw material via a solid state reaction.

Fig. 3 presents XRD patterns of the pristine $Li[Li_{0.23}Ni_{0.15}Mn_{0.62}]O_2$ and the charged/discharged cathode material. The pristine $Li[Li_{0.23}Ni_{0.15}Mn_{0.62}]O_2$ has a layered structure with an wide interlayer spacing (d_{001} = 0.47 nm, in Fig. 3a). Either the charged cathode or the discharged one has the similar peaks at ~ 18.5°, 37.8°, and 44.5° (Figs. 3b and 3c). So the cathode material has a stable framework for lithium extraction and insertion during cycling. The broadening peaks in Figs. 3b and 3c indicate the decreasing crystallite sizes after cycling. The discharged sample show two diffraction peaks being attributed to the spinel $LiMn_2O_4$ and monoclinic $LiMnO_2$, respectively.

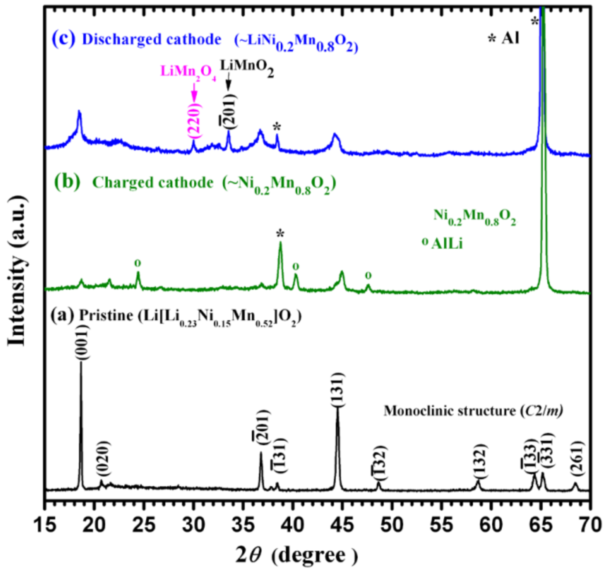

Figure 3. XRD patterns for: (a) pristine $Li[Li_{0.23}Ni_{0.15}Mn_{0.62}]O_2$, (b) charged cathode after 50 charges, and (c) discharged cathode after 20 discharges. The diffraction peaks of aluminum result from the current collectors.

Fig. 4 shows the HRTEM images of the cycled cathode material. Both the charged and the discharged cathode materials still contain crystallites. It proves that the cathode material keep a stable framework during cycling. The interlayer spacings of 0.18 and 0.47 nm respectively correspond to the diffraction peaks located on 18.5 ° and 44.5 ° shown in Fig. 3.

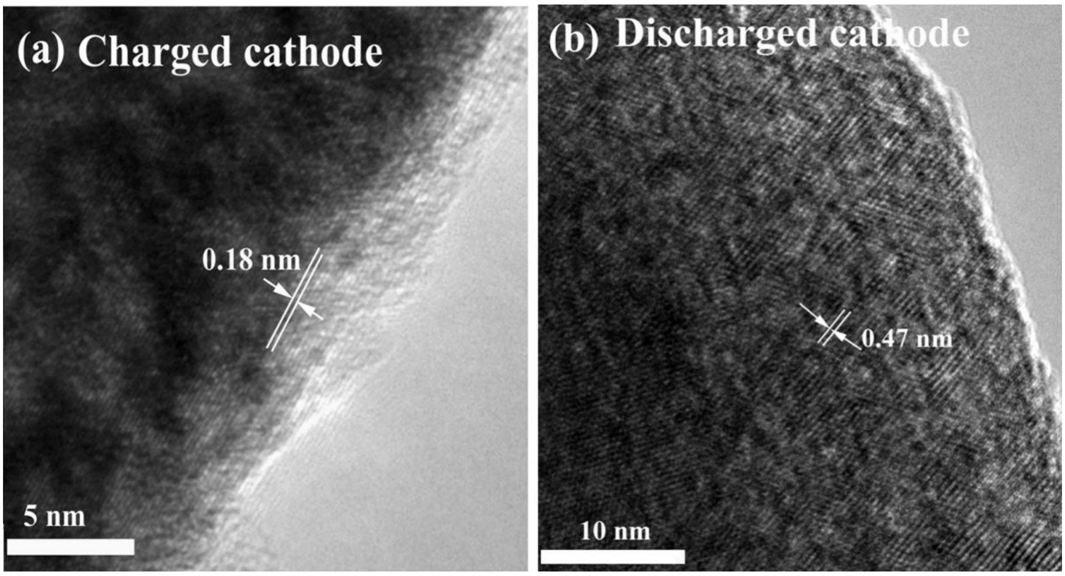

Figure 4. HRTEM imagines for: (a) the charged cathode material after the initial charge, and (b) the discharged cathode material after the initial discharge.

Fig. 5a shows the charge–discharge curves of $Li[Li_{0.23}Ni_{0.15}Mn_{0.62}]O_2$ as cathode material. Obviously, the 1st charge curve consists of a sloping voltage region and a unique high voltage plateau.

The sloping voltage region reflects a charge capacity of 156 mAh g^{-1} realized between 3.74 and 4.36 V. The voltage plateau starts from 4.36 V, passes through 4.52 V, and ends at 4.8 V. It contributes a charge capacity of 205 mAh g^{-1}. So the 1st charge delivers a total capacity of 361 mAh g^{-1}. However, there only is a capacity of 221 mAh g^{-1} during the 1st discharge. The capacity loss of 140 mAh g^{-1} is attributed to the structural rearrangement of cathode material. The 2nd charge curve shows an uncommon short plateau at 4.5 V, indicating a complementary structural rearrangement. After the first two cycles, the charge/discharge curves exhibit the similar profiles. Their starting charge voltages descend to ~ 3.0 V, and no obvious high voltage plateaus are found.

As shown in Fig. 5b, in the d*Q*/d*V* curve of the initial charge, the oxidation peak at 3.74 V is attributed to the oxidation of Ni^{2+} into Ni^{4+} as lithium extracts from $LiNi_{0.5}Mn_{0.5}O_2$ component [3]. The oxidation peak at 4.07 V possibly originates from delithiation of the residual Mn^{3+} ions in the pristine sample, such as spinel $LiMn_2O_4$. It was reported that a synthetic $Li[Li_{0.2}Mn_{0.61}Ni_{0.18}Mg_{0.01}]O_2$ contains a certain amount of Mn^{3+} (average Mn oxidation state: +3.75) and $LiMn_2O_4$ is oxidized at a voltage plateau at 4 V [14]. The steep peaks at ~ 4.52 V only appear in the first two charge curves, and are related with the material structural rearrangement caused by irreversible oxygen loss and lithium extraction.

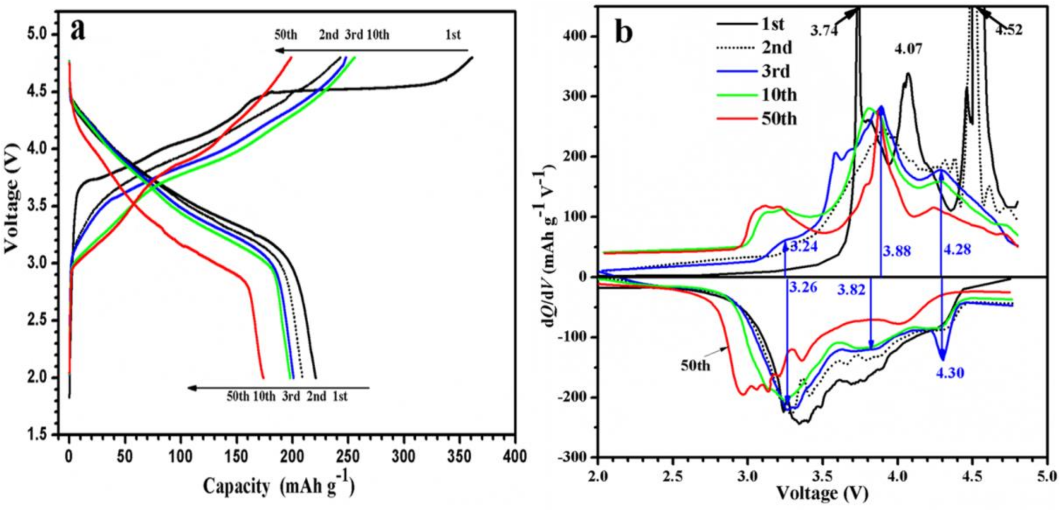

Figure 5. (a) Charge/discharge curves and (b) d*Q*/d*V* (vs. voltage) curves of the Li/$LiPF_6$ (EC-DMC)/$Li[Li_{0.23}Ni_{0.15}Mn_{0.62}]O_2$ cell between 2.0 and 4.8 V at a current density of 20 mA g^{-1}.

During the 3rd cycle, the d*Q*/d*V* curves show three redox couple peaks at 3.24 V/3.26 V, 3.88 V/3.82 V, and 4.28 V/4.30 V. The similar three-couple peaks had been reported in literatures [8, 15], and are used to explain the delithiation/lithiation mechanism of lithium-rich layered oxide.

Based on the experimental results and the previous research of Kang *et al.* [16, 17], we propose a delithiation/lithiation mechanism for $Li[Li_{0.23}Ni_{0.15}Mn_{0.62}]O_2$. $Li[Li_{0.23}Ni_{0.15}Mn_{0.62}]O_2$ is written as $0.9Li[Li_{1/3}Mn_{2/3}]O_2 \cdot 0.4LiNi_{0.5}Mn_{0.5}O_2$ for facile discussing.

During the 1st charge, there are three oxidation reactions (1)–(3), being respectively reflected by the oxidation peaks at 3.74, 4.07, and 4.52 V in Fig. 3b.

$LiNi_{0.5}Mn_{0.5}O_2 \rightarrow Li^+ + Ni_{0.5}Mn_{0.5}O_2 + e^-$ (1)
$LiMn_2O_4 \rightarrow Li^+ + 2\ MnO_2 + e^-$ (2)
$Li[Li_{1/3}Mn_{2/3}]O_2 \rightarrow 4/3\ Li^+ + 2/3\ MnO_2 + 2O\cdot + 1/3\ e^-$ (3)

The sloping voltage region mainly reflects the capacity caused by reactions (1) and (2), and the high voltage plateau reflects the capacity caused by reaction (3). Mn^{3+} is oxidized into Mn^{4+} via reaction (2). The initial capacity loss is caused by the simultaneous irreversible lithium extraction and oxygen loss via reaction (3) at ~ 4.52 V. The highly reactive oxygen atoms can react with electrolyte and form solid-electrolyte interphase (SEI) layers.

$Li[Li_{0.23}Ni_{0.15}Mn_{0.62}]O_2$ is rearranged into $Ni_{0.2}Mn_{0.8}O_2$ after full delithiation.

During the initial discharge, $Ni_{0.2}Mn_{0.8}O_2$ is lithiated into $LiNiMnO_2$. There are three suggested reduction reactions (4)–(6), being reflected by three reduction peaks at 4.30, 3.82, and 3.26 V.

$0.4\ Li^+ + Ni_{0.2}Mn^{4+}{}_{0.8}O_2 + 0.4\ e^- \rightarrow Li_{0.4}Ni_{0.2}Mn^{3+}{}_{0.4}Mn^{4+}{}_{0.4}O_2$ (4)
$0.4\ Li^+ + Li_{0.4}Ni^{4+}{}_{0.2}Mn_{0.8}O_2 + 0.4\ e^- \rightarrow Li_{0.8}Ni^{2+}{}_{0.2}Mn_{0.8}O_2$ (5)
$0.2\ Li^+ + Li_{0.8}Ni_{0.2}Mn^{3+}{}_{0.4}Mn^{4+}{}_{0.4}O_2 + 0.2\ e^- \rightarrow LiNi_{0.2}Mn^{3+}{}_{0.6}Mn^{4+}{}_{0.2}O_2$ (6)

During the 3rd charge from 2.0 to 4.8 V, there are three reverse reactions (7)−(9) corresponding to reactions (6)−(5):

$LiNi^{2+}{}_{0.2}Mn^{3+}{}_{0.6}Mn^{4+}{}_{0.2}O_2 \rightarrow 0.2\ Li^+ + Li_{0.8}Ni^{2+}{}_{0.2}Mn^{3+}{}_{0.4}Mn^{4+}{}_{0.4}O_2 + 0.2\ e^-$ (7)
$Li_{0.8}Ni^{2+}{}_{0.2}Mn^{4+}{}_{0.8}O_2 \rightarrow 0.4\ Li^+ + Li_{0.4}Ni^{4+}{}_{0.2}Mn^{4+}{}_{0.8}O_2 + 0.4\ e^-$ (8)
$Li_{0.4}Ni^{4+}{}_{0.2}Mn^{3+}{}_{0.4}Mn^{4+}{}_{0.4}O_2 \rightarrow 0.4\ Li^+ + Ni^{4+}{}_{0.2}Mn^{4+}{}_{0.8}O_2 + 0.4e^-$ (9)

After the reactions, the valence state of all Ni and 3/4 Mn changes from +2 to +4. Whereas, 1/4 Mn keeps unchanged tetravalent state. Differing from the 1st charge curve starting from ~ 3.6 V, the other charge curves start from a lower voltage at ~ 3.0 V. It reflects the conversion of partial Mn^{4+} via reaction (4), which close to the value of 3.1 V reported in $LiMnO_2$ charging [2].

In summary, the $Li[Li_{0.23}Ni_{0.15}Mn_{0.62}]O_2$ is rearranged into $LiNi_{0.2}Mn_{0.8}O_2$ after the irreversible oxygen loss and extraction of “rich lithium” at ~ 4.52 V during the initial charges, i.e.

$Li[Li_{0.23}Ni_{0.15}Mn_{0.62}]O_2 \rightarrow Ni_{0.2}Mn_{0.8}O_2 + 1.6\ Li^+ + 0.6\ O + 1.6\ e^-$ (10)

After the rearrangement, the cathodes’ high capacities during cycling originate from the reversible conversions between $Ni_{0.2}Mn_{0.8}MnO_2$ and $LiNi_{0.2}Mn_{0.8}O_2$, i.e.

$LiNi^{2+}{}_{0.2}Mn^{3+}{}_{0.6}Mn^{4+}{}_{0.2}O_2 \leftrightarrow Li^+ + Ni^{4+}{}_{0.2}Mn^{4+}{}_{0.8}O_2 + e^-$ (11)

Both $Ni_{0.2}Mn_{0.8}MnO_2$ and $LiNi_{0.2}Mn_{0.8}O_2$ possess a stable layered structure with similar interlayer spacing of ~ 0.47 nm, which is reflected by the peaks at ~18.5° in Figs. 3b and 3c. It is well known that $LiCoO_2$ loses its rechargeable behavior caused by irreversible structure change after full delithiation. 1/4 Mn with an unchanged tetravalent state weakens the Jahn-Teller effect of Mn^{3+} and benefits the stabilization of the charged/discharged cathode.

The above-mentioned mechanism is better in explaining the high capacity and stability of lithium-rich layered oxide. In literatures [9, 18, 19], the cathodes' high capacities are partially attributed to the reversible valence state changes involving either oxygen molecules at the electrode surface or coordinated O^{2-} in the crystals. Some researchers thought that Mn keeps a stable tetravalent state even in charged cathodes [19], while some others argued that partial Mn is activated after the structural rearrangement caused by Li_2O removal [9].

Additionally, it is well-accepted that the lithium-rich layered oxide consists of transition metal layers and lithium layers [12, 13]. The transition metal layer is built by MO_6 (M = Mn, Ni, Li) octahedra. Not only all Mn and Ni but also partial Li, i.e. the "rich lithium", locates in the transition metal layers. It was reported that some transition metal atoms (~ 5%) migrate from the transition metal layers into the lithium layers during the 1st charge [9, 20]. In this work, for $0.9Li[Li_{1/3}Mn_{2/3}]O_2{\cdot}0.4LiNi_{0.5}Mn_{0.5}O_2$, 1/4 lithium of $Li[Li_{1/3}Mn_{2/3}]O_2$ component is located in transition metal layers, and the rest 3/4 lithium in lithium layers. We think that some transition metal atoms migrate into the lithium layers after structural rearrangement during the first charge. The migrated transition metal atoms play the role as supports (or pillars) between the transition metal layers and can stabilize the layered structure even if all lithium being extracted.

According to the proposed mechanism, the expected capacity of $Li[Li_{(1-2x)/3}Ni_xMn_{(2-x)/3}]O_2$ ($0 < x < 0.5$) is calculated and shown in Fig. 6. With increasing x value from 0 to 0.5, the expected first charge capacity decreases from 459 to 280 mAh g^{-1}. Nevertheless, the reversible capacity increase from 230 to 280 mAh g^{-1}.

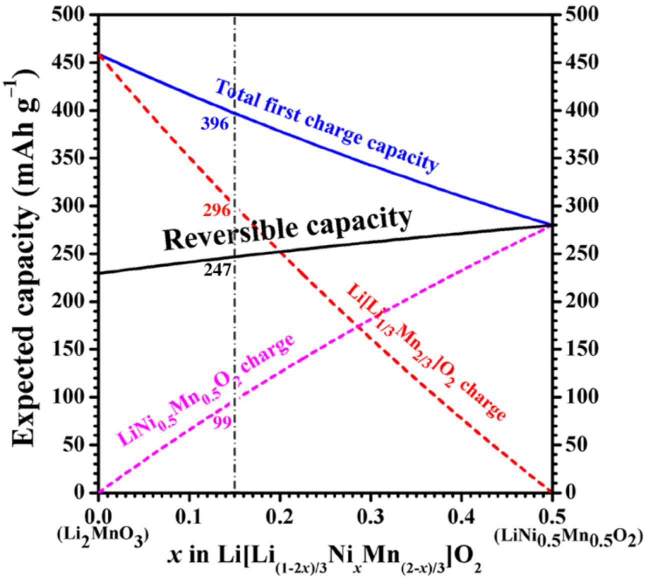

Figure 6. Predicted capacity (*vs.* x) of lithium-rich layered oxide $Li[Li_{(1-2x)/3}Ni_xMn_{(2-x)/3}]O_2$ ($0 < x < 0.5$). The two inclined dotted lines respectively indicate the capacities of the components $Li[Li_{1/3}Mn_{2/3}]O_2$ and $LiNi_{0.5}Mn_{0.5}O_2$ during the 1st charge. The vertical short dash line labels the capacities of the tested $Li[Li_{0.23}Ni_{0.15}Mn_{0.62}]O_2$.

The predicted results can be used to explain the experimental results in this work and literature, as shown in Table 1. The predicted initial charge capacity and reversible capacity are 396 and 247 mAh g^{-1}, which close the experimental values of 361 and 221 mAh g^{-1}, respectively. The tested $Li[Li_{0.23}Ni_{0.15}Mn_{0.62}]O_2$ sample delivers a capacity of 156 mAh g^{-1} in the sloping region below 4.36 V, which exceeds the predicted value (99 mAh g^{-1}) resulting from the charging of the component $LiNi_{0.5}Mn_{0.5}O_2$, i.e. reaction (1). We think that the excess capacity is caused by the delithiation of the residual Mn^{3+}-containing components, such as $LiMn_2O_4$, via reaction (2)

Table 1. Predicted and experimental capacity of $Li[Li_{(1-2x)/3}Ni_xMn_{(2-x)/3}]O_2$ ($0 < x < 0.5$)

Cathode Material	x	Predicted Capacity (mAh g^{-1})		Experimental Capacity (mAh g^{-1})		Ref.
		Initial Charge	Reversible Charge	Initial Charge	Reversible Charge/discharge	
$Li[Li_{1/3}Mn_{2/3}]O_2$	0	459	229	124	73	[23]
				323	243	[26]
				336	148	[28]
$Li[Li_{0.23}Ni_{0.15}Mn_{0.62}]O_2$	0.15	396	247	272	~ 219	[21]
				361	221	This work
$Li[Li_{0.2}Ni_{0.2}Mn_{0.6}]O_2$	0.2	380	253	353	240	[23]
				–	243	[24]
				~ 322	~ 241	[25]
$Li[Li_{1/9}Ni_{1/3}Mn_{5/9}]O_2$	1/3	330	268	~ 280	220	[1]
$LiNi_{0.5}Mn_{0.5}O_2$	0.5	280	280	240	194	[23]
				–	~ 150	[29]
				275	> 180	[30]
				~255	~ 170	[31]
				210	~ 180	[32]

The predicted results also coincide with previous investigations. Especially, the short sloping voltage regions with an initial charge capacity between 90 and 150 mAh g^{-1} often appear in literature [16, 21−25]. As a start end material, Li_2MnO_3, i.e. $Li[Li_{1/3}Mn_{2/3}]O_2$, has an predicted initial charge capacity of 459 mAh g^{-1}, but its predicted reversible capacity is just a half value (229 mAh g^{-1}) due to the serious oxygen loss. It was reported that nanosized Li_2MnO_3 delivers a capacity of 243 mAh g^{-1} between 2.0 and 4.3 V during the 1st discharge [26]. But its discharge capacity decays to ~ 160 mAh g^{-1} after 25 cycles. Generally, Li_2MnO_3 has worse rate capability and cyclic performance due to its low electronic conductivity and unstable structure [27, 28]. At the other end, $LiNi_{0.5}Mn_{0.5}O_2$ has a high predicted reversible capacity of 280 mAh g^{-1} [29]. However, its experimental capacities are often less than 180 mAh g^{-1} with worse stability [30−32].

Generally, the lithium-rich layered oxide $Li[Li_{(1-2x)/3}Ni_xMn_{(2-x)/3}]O_2$ ($0.15 < x < 1/3$) cathode often exhibits a high capacity (> 210 mAh g^{-1}) after its structural rearrangement (Table 1). Its high capacity is attributed to its stable structures in both charged and discharged states, modified electronic conductivity, and facilely synthesized pure phases.

Experimentally, the discharge capacity of $Li[Li_{0.23}Ni_{0.15}Mn_{0.62}]O_2$ decreases during cycles. The discharge capacity is 174 mA g^{-1} in the 50th cycle, which means ~ 0.70 lithium ion insertion. The capacity decay is mainly attributed to the continual oxygen loss at high voltages during charging, which induces the Li_2MnO_3 component changing into spinel $LiMn_2O_4$. In Figure 4b, the redox couple potential at ~ 3.0 V in the 50th cycle is attributed to the formation of $LiMn_2O_4$. The formation of spinel $LiMn_2O_4$ induces a two-phase structure, which affects the lithium transfer and capacity of the cathodes.

4. CONCLUSIONS

In this work, we investigated the formation of monoclinic $Li[Li_{0.23}Ni_{0.15}Mn_{0.62}]O_2$ via *in situ* XRD analyses. $Li[Li_{0.23}Ni_{0.15}Mn_{0.62}]O_2$ was used as the cathodes for lithium-ion batteries, and its delithiation/lithiation mechanism is discussed. We suggested that $Li[Li_{0.23}Ni_{0.15}Mn_{0.62}]O_2$ is rearranged into $Ni_{0.2}Mn_{0.8}MnO_2$ after an irreversible oxygen loss and extraction of "rich lithium" during the initial charge, i.e., $Li[Li_{0.23}Ni_{0.15}Mn_{0.62}]O_2 \rightarrow Ni_{0.2}Mn_{0.8}O_2 + 1.6\ Li^+ + 0.6\ O + 1.6\ e^-$. The cathodes have high capacities result from the following conversions between $Ni_{0.2}Mn_{0.8}MnO_2$ and $LiNi_{0.2}Mn_{0.8}O_2$, i.e., $Li^+ + Ni_{0.2}Mn_{0.8}O_2 + e^- \leftrightarrow LiNi_{0.2}Mn_{0.8}O_2$. The cathode materials can keep a stable framework during cycling due to two suggested reasons: (1) some transition metal atoms migrate into the lithium layers during the structure rearrangement and play as the supports between transition metal layers; (2) partial Mn in a stable tetravalent state weakens the Jahn-Teller effect of Mn^{3+}. According to the suggested mechanism, the predicted reversible capacity of lithium-rich layered oxides $Li[Li_{(1-2x)/3}Ni_xMn_{(2-x)/3}]O_2$ ($0 < x < 0.5$) increases from 229 to 280 mAh g^{-1} with increasing x value. The continual oxygen losses at high charge voltages results in the formation of spinel $LiMn_2O_4$, which corresponds to the capacity fading of the cathodes during cycling.

ACKNOWLEDGEMENTS
This research was funded by the National Nature Science Foundation of China (NSFC 5117260) and the Nature Science Foundation of Tianjin City (No. 14RCHZGX00859 and No. 14JCTPJC00484).

References

1. Z. Lu, D. D. MacNeil and J. R. Dahn, *Electrochem. Solid State Lett.* 4 (2001) A191.
2. M. S. Whittingham, *Chem. Rev.* 104(10) (2004) 4271.
3. M. Jiang, B. Key, Y. S. Meng and C.P. Grey, *Chem. Mater.* 21 (2009) 2733.
4. S. H. Kang, Y. K. Sun and K. Amine, *Electrochem. Solid State Lett.* 6 (2003) A183.
5. Z. Q. Deng and A. Manthiram, *J. Phys. Chem. C* 115 (2011) 7097.
6. A. Manthiram, J. C. Knight, S. T. Myung, S. M. Oh, Y. K. Sun, *Adv. Energy Mater.* 6 (2016) 1501010.

7. J. X. Wang, L. Wang, X. M. He, J. J. Li, Z. J. Dai and J. L. Wang, *Int. J. Electrochem. Sci.* 11 (2016) 333.
8. R. M. Gu, S. Y. Yan, S. Sun, C. Y. Wang and M. W. Li, *J. Solid State Electrochem.* 19 (2015) 1659.
9. N. Yabuuchi, K. Yoshii, S. T. Myung, I. Nakai and S. Komaba, *J. Am. Chem. Soc.* 133 (2011) 4404.
10. F. S. Feng, H. S. Fang, B. Yang, W. H. Ma and Y. B. Dai, *Int. J. Electrochem. Sci*. 9 (2014) 6852.
11. K. A. Jarvis, Z. Deng, L.F . Allard, A. Manthiram and P. J. Ferreira, *Chem. Mater.* 23 (2011) 3614.
12. A. K. Shukla, Q. M. Ramasse, C. Ophus, H. Duncan, F. Hage and G. Chen, *Nat. Commun.* 6 (2015) 8711
13. X. D. Xiang and W. S. Li, *Electrochim. Acta* 133 (2014) 422.
14. L. Simonin, J. F. Colin, V. Ranieri, E. Canévet, J. F. Martin, C. Bourbon, C. Baehtz, P. Strobel, L. Daniel and S. Patoux, *J. Mater. Chem.* 22 (2012) 11316.
15. J. Hong, D. H. Seo, S. W. Kim, H. Gwon, S. T. Oh, K. Kang, *J. Mater. Chem.* 20 (2010) 10179.
16. S. H. Kang and M. M. Thackeray, *Electrochem. Commun.* 11 (2009) 748.
17. D. P. Abraham, R. D. Twesten, M. Balasubramanian, I. Petrov, J. McBreen and K. Amine, *Electrochem. Commun.* 4 (2002) 620.
18. A. Ito, Y. Sato, T. Sanada, M. Hatano, H. Horie and Y. Ohsawa, *J. Power Sources* 196 (2011) 6828.
19. M. Oishi, C. Yogi, I. Watanabe, T. Ohta, Y. Orikasa, Y. Uchimoto and Z. Ogumi, *J. Power Sources* 276 (2015) 89.
20. A. Ito, K. Shoda, Y. Sato, M. Hatano, H. Horie and Y. Ohsawa, *J. Power Sources* 196 (2011) 4785.
21. J. H. Kim, S. H. Choi, M. Y. Son, M. H. Kim, J. K. Lee and Y. C. Kang, *Ceramics International* 39 (2012) 331.
22. S. J. Han, B. Qiu, Z. Wei, Y. G. Xia and Z. P. Liu, *J. Power Sources* 268 (2014) 683.
23. S. Hy, J. H. Cheng, J. Y. Liu, C. J. Pan, J. Rick, J. F. Lee, J. M. Chen and B. J. Hwang, *Chem. Mater.* 26 (2014) 6919.
24. Y. Li, C. Wu, Y. Bai, L. Liu, H. Wang, F. Wu, N. Zhang and Y. F. Zou, *ACS Appl. Mater. Interfaces* 8 (2016) 18832.
25. K. Luo, M. R. Roberts, R. Hao, N. Guerrini, E. Liberti, C. S. Allen, A. I. Kirkland and P. G. Bruce, *Nano Letters* 16 (2016) 7503.
26. G. R. Liu and S. C. Zhang, *Int. J. Electrochem. Sci.* 11 (2016) 5545.
27. S. F. Amalraj, L. Burlaka, C. M. Julien, A. Mauger, D. Kovacheva, M. Talianker, B. Markovsky and D. Aurbach, *Electrochim. Acta* 123 (2014) 395.
28. P. J. Phillips, J. Bareno, Y. Li, D. P. Abraham and R. F. Klie, *Adv. Energy Mater.* 5 (2015) 1501252.
29. T. Ohzuku and Y. Makimura, *Chem. Lett.* 8 (2001) 744.
30. J. Bréger, Y. S. Meng, Y. Hinuma, S. Kumar, K. Kang, Y. Shao-Horn, G. Ceder and C. P. Grey, *Chem. Mater.* 18 (2006) 4768.
31. Y. M. Liu, B. L. Chen, F. Cao, X. Z. Zhao and J. K. Yuan, *J. Mater. Chem.* 21 (2011) 10437.
32. L. Shi, W. T. Xie, Q. S. Ge, S. Wang, D. Chen, L. S. Qin, M. Q. Fan, L. Q. Bai, Z. Chen and H. Y. Shen, *Int. J. Electrochem. Sci.* 10 (2015) 4696.